Crystal Structure of Arp2/3 Complex

Robert C. Robinson,*† Kirsi Turbedsky,* Donald A. Kaiser, Jean-Baptiste Marchand,‡ Henry N. Higgs,§ Senyon Choe, Thomas D. Pollard‖¶

We determined a crystal structure of bovine Arp2/3 complex, an assembly of seven proteins that initiates actin polymerization in eukaryotic cells, at 2.0 angstrom resolution. Actin-related protein 2 (Arp2) and Arp3 are folded like actin, with distinctive surface features. Subunits ARPC2 p34 and ARPC4 p20 in the core of the complex associate through long carboxyl-terminal α helices and have similarly folded amino-terminal α/β domains. ARPC1 p40 is a seven-blade β propeller with an insertion that may associate with the side of an actin filament. ARPC3 p21 and ARPC5 p16 are globular α-helical subunits. We predict that WASp/Scar proteins activate Arp2/3 complex by bringing Arp2 into proximity with Arp3 for nucleation of a branch on the side of a preexisting actin filament.

Arp2/3 complex, a stable assembly of two actin-related proteins and five novel protein subunits (*1*), is the heart of the machine that generates the branched actin filament network responsible for pushing forward the leading edge of motile eukaryotic cells (*2, 3*). The complex promotes nucleation of actin filaments as 70° branches on the sides of older filaments (*4–6*). The complex is inactive until stimulated jointly by interaction with WASp/Scar proteins or other nucleation-promoting factors (*7–11*) and with the side of a preexisting filament (*5–7*). The filament not only provides the base or "mother filament" for the branch but also acts as a secondary activator of nucleation. WASp/Scar proteins require activation through chemotactic signaling pathways that guide the direction of cellular movement (*12, 13*). WASp promotes binding of Arp2/3 complex to the side of a preexisting filament (*14*) and may deliver the first actin subunit to the fast-growing barbed end of the new filament (*15, 16*).

Conservation of the sequences of the seven subunits of this large (220 kD) complex from protozoa to mammals (*17–19*) suggests that the encoding genes arose early in the eukaryotic lineage and have been tightly conserved by functional constraints for more than a billion years. Primary sequences revealed homology of the Arps to actin and of subunit p40 (gene name *ARPC1*) to β-propeller proteins, but the other four subunits in the complex (genes named *ARPC2* through *ARPC5*) share little sequence homology to known proteins. Homology models of the structures of Arp2 and Arp3 based on the structure of actin suggested that they might form a dimer that would cap the slow-growing pointed end of an actin filament and initiate growth of a new filament in the fast-growing barbed direction (*19*). Both predictions were verified (*4*). Electron microscopy (*4, 20, 21*) and chemical cross-linking (*20, 22*) revealed the overall shape of the complex and subunit nearest neighbors.

Our crystal structure of bovine Arp2/3 complex at 2.0 Å resolution reveals the structure of each subunit as well as their relationships. This structure suggests that activation involves a concerted movement of several subunits, allowing Arp2 and Arp3 to form a nucleation site for the growth of a new actin filament. A contact between ARPC1 p40 and Arp3 in an adjacent complex in the crystal is a possible anchor for the complex on the side of an actin filament.

Structure determination. Crystals of bovine Arp2/3 complex in space group $P2_12_12_1$ diffracted to a resolution of 2.0 Å (Table 1). We calculated the electron density map from a multiwavelength anomalous diffraction data set collected at three wavelengths from a crystal with 34 platinum atoms per asymmetric unit. This experimental phase map allowed us to identify all seven subunits and build a preliminary model with 65% of the 1980 residues. Several rounds of refinement against native data followed by rebuilding resulted in the present model with 1709 residues and 1881 waters (R_{free} = 24.9%). Weak electron density indicates that subdomains 1 and 2 of Arp2 are highly flexible. We used a model of actin to trace the backbone for this half of Arp2 but did not include it in the refined model. Instead, we show a polyalanine model of actin for subdomains 1 and 2 of Arp2 to indicate their orientation relative to subdomains 3 and 4.

Overall shape of the Arp2/3 complex and arrangement of the seven subunits. The Arp2/3 complex is a flat ellipsoid about 150 Å long, 140 Å wide, and 70 to 100 Å thick [Fig. 1 and Web fig. 1 (*23*)]. A dimer of subunits ARPC2 p34 and ARPC4 p20 (two shades of blue in the figures) form a C-shaped clamp that cradles the Arp subunits (orange and red). Extensive interactions with p34 bury 2100 Å^2 of the surface of p20 [Web table 1 (*23*)]. Contacts with both Arps, ARPC1 p40, and ARPC5 p16 bury an additional 3300 Å^2 of the surface of p20. p34 makes extensive contacts (3862 Å^2 of surface) with p20 and with Arp3, which p34 embraces between its NH_2-terminal α/β1 domain and its COOH-terminal helix. The NH_2-terminal α/β2 domain of p34 and subunit ARPC1 p40 reinforce the top and bottom of this clamp. Experiments with yeast (*24*) had suggested critical roles for p20 and p34. The flat Arp subunits lie end to end in this clamp, tilted about 40° from the plane defined by p16, p20, p34, and p40. The Arps are splayed apart slightly, accounting for the cleft observed in electron micrographs of shadowed specimens (*4, 20*). This separation thins one side of the ellipsoid, creating a slight indentation featured in reconstructions from cryo-electron micrographs (*21*). Subunits ARPC3 p21 and ARPC5 p16 decorate the edges of the structure. Both p21 and p40 have large basic patches (Fig. 1C). The arrangement of subunits agrees well with extensive chemical cross-linking experiments and with one, but not all, reported two-hybrid interactions (*22, 25*).

Structures of the actin-related proteins. Arp3 resembles the actin fold to such a degree that the actin backbone fits reasonably well into the experimental map, with the exception that the central cleft is spread open about 12° further than actin and lacks a bound nucleotide (Fig. 2C). An extensive network of bound waters replaces the nucleotide in this cleft. Although Arp3 has most of the residues that interact with adenosine triphosphate (ATP) in actin (*26*), the affinity is lower (*27*) so that nucleotide is lost during purification and crystallization in buffers without free ATP.

Arp3 has 42 more residues than actin, most of which are found in four insertions that extend surface loops and adjacent elements of secondary structure. We refer to four subdomains, as originally defined for

Structural Biology Laboratory, Salk Institute for Biological Studies, 10010 North Torrey Pines Road, La Jolla, CA 92037, USA.

*These authors contributed equally to this work.
†Present address: Department of Medical Biochemistry and Microbiology, Uppsala University, Uppsala, Sweden.
‡Present address: Avidis, Biopole Clermont-Limagne, 63 360 Saint Beauzire, France.
§Present address: Department of Biochemistry, Dartmouth College, Hanover, NH 03755, USA.
‖Present address: Department of Molecular, Cellular, and Developmental Biology, Yale University, New Haven, CT 06520, USA.
¶To whom correspondence should be addressed. E-mail: thomas.pollard@yale.edu

actin (Fig. 2A). The first insert, Gln^{46} to Cys^{54}, extends a long surface loop, most of which is poorly represented in the electron density map. This loop, corresponding to the deoxyribonuclease (DNase) binding loop of actin, is exposed to solvent near the interface of subdomain 2 of Arp3 with p34. The second insert, Thr^{154} to Arg^{161}, adds seven residues to the loop between the end of the long helix connecting subdomain 2 to the core β sheet of subdomain 3. This loop is exposed to solvent on the back side of Arp3 in our standard view. The third insert from sequence alignments, Ser^{263} to Phe^{267}, is used for the structural insert 260–264 that extends two antiparallel β strands at the top of subdomain 4. The fourth insert, Val^{347} to Leu^{358}, adds almost two turns to a long α helix 9 and extends the following loop at the lower left corner of subdomain 3. This longer helix and loop form a principal contact with p21.

The experimental map had strong density for subdomains 3 and 4 of Arp2, but very little for subdomains 1 and 2. Density sufficient to identify helices and thus orient subdomains 1 and 2 appeared weakly only after three rounds of refinement. Because this density was too weak to trace the entire chain through both subdomains, we show a polyalanine backbone model in their place.

Subdomains 3 and 4 of Arp2 are similar to actin, sharing all elements of secondary structure. However, the central cleft is open by about 18° compared with actin and lacks a bound nucleotide. Although most of the residues of actin that interact with ATP are conserved in Arp2 (*26*), the affinity is low (*27*), so bound ATP was lost during purification and crystallization. Arp2 has 19 extra residues compared with actin. The only large insert, Tyr^{325}–Glu^{335}, extends helix 9 and the following loop in the lower left corner of subdomain 3. This insert is structurally equivalent to the fourth insert of Arp3. This helix interacts with the NH_2-terminus of p16 on the back side of our standard view of the complex.

Structures of ARPC2 p34 and ARPC4 p20. ARPC2 p34 and ARPC4 p20 form a dimer at the heart of the Arp2/3 complex. The folds of residues 1 to 114 and 115 to 236 of p34 are similar to each other and to the NH_2-terminal 127 residues of p20 (Fig. 3, C and D). These α/β domains start with a four-turn helix followed by an antiparallel β sheet of five strands, with an α helix inserted between strands 3 and 4 and completed by a short helix. Although similar in structure, structure-based alignments of the sequences of these domains revealed few identical residues: p34 α/β1 and α/β2 have only seven identical residues, p34 α/β1 and p20 α/β have 14 identical residues, and p34 α/β2 and p20 α/β have nine identical residues. A search for proteins with folds similar to these α/β domains yielded no matches.

Long COOH-terminal helices of 43 residues (p34) and 38 residues (p20) associate with each other in an antiparallel fashion with a crossing angle of about –20°. These helices are loosely packed compared with true antiparallel coiled coils. The interface includes two cavities: the larger one surrounded by p20 156/160 and p34 254/258, and the smaller one surrounded by p20 145 and p34 265/269. The interface between the helices is formed by hydrophobic residues and two salt bridges, but these residues are not spaced in a regular heptad repeat or packed in a knob-in-hole fashion (*28*).

Structure of ARPC1 p40. ARPC1 p40 (Fig. 3E) is a WD40 β-propeller protein with seven blades each consisting of 42 to 96 residues folded into four β strands. Like G protein β subunits, the NH_2-terminal strand of the polypeptide completes blade 7 as its D strand before the second strand initiates blade 1 as strand A. Unlike β subunits, the polypeptide chain starts with this strand rather than with an NH_2-terminal extension. Blades 1 to 4 have tryptophan in the W position at the distal end of strand A, and blades 5 to 7 have phenylalanine in this position. None of these W positions of p40 is followed by the aspartic acid that gave β propeller their names as "WD repeat" proteins. An insert of 23 residues between strands C and D of blade 4 is exposed to solvent on the lower surface of p40 in our standard orientation. Unlike G protein β subunits, p40 has an insert of 35 residues between blades 6 and 7. Residues 297 to 309 of this loop are ordered, with residues 297 to 305 forming a short helix that interacts with Arp3 in an adjacent complex related by (–x, ½ + *y*, ½ – *z*) symmetry [Web fig. 2 (*23*)]. Both connections of this helix to the rest of p40 (residues 289 to 296 and 310 to 319) are disordered. The top faces of all seven blades interact extensively with the NH_2-terminal α/β domain of p20. The top of blades 4 and 5 interact with helix 138–148 of

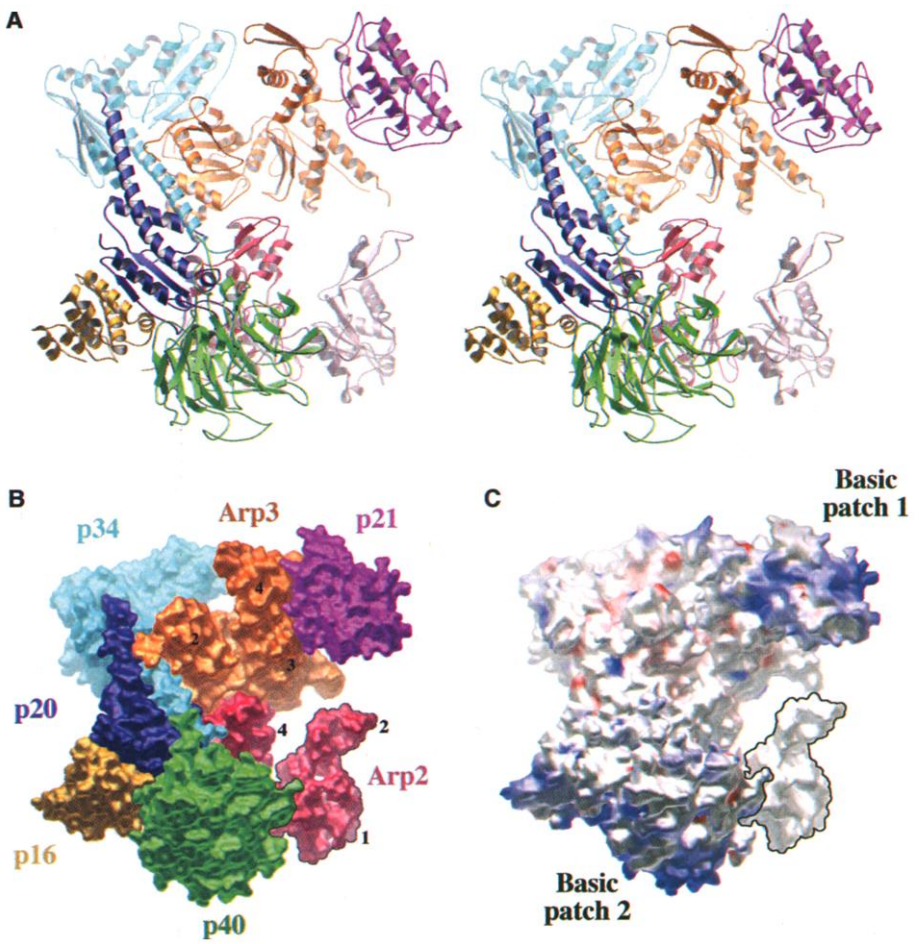

Fig. 1. Atomic structure of bovine Arp2/3 complex viewed from the front. This standard view shows Arp2 in the classic actin orientation. (**A**) Stereopair of ribbon diagrams (*40*–*42*). Color codes for subunits: Arp3, orange; Arp2, red for subdomains 3 and 4, gray-red for the actin backbone model of subdomains 1 and 2; p40, green; p34, light blue; p20, dark blue; p21, magenta; p16, yellow. (**B**) Space-filling model with the subdomains of Arp2 and Arp3 indicated (*43*). (**C**) Space-filling model with the electrostatic potential indicated with blue as positive and red as negative (*43*). Both p21 and p40 have strongly basic surface patches. The actin backbone model of Arp2 subdomains 1 and 2 is outlined in (B) and (C).

p16 and blade 4 with the NH_2-terminal extension of p16. The bottom face of p40 has an extensive patch of basic residues shown in the electrostatic representation of the molecular surface [Fig. 1C and Web fig. 1 (*23*)].

Structures of ARPC3 p21 and ARPC5 p16. ARPC3 p21 (Fig. 3B) is a bundle of four substantial α helices connected by some long surface loops. Two long NH_2-terminal loops interrupted by two short antiparallel β strands lead, at residue 52, to three turns of helix 1. A short loop of nine residues connects to five turns of helix 2, followed by a short loop and three turns of helix 3. A surface loop of 22 residues leads to six turns of helix 4. The final loop of 27 residues includes one turn of α helix. The surface loops form an extensive hydrophobic interface with subdomains 3 and 4 of Arp3 bordered by salt bridges. A search for proteins with similar folds yielded no matches.

ARPC5 p16 (Fig. 3A) begins with a particularly long NH_2-terminal extension that winds around and interacts extensively with p20, p40, and Arp2 and ends with a bundle of seven α helices that interacts with p20 and p40. This NH_2-terminal extension may simply reinforce the interactions among Arp2, p40, and p20 or relay conformational changes between these subunits. p16 protrudes from the plane of the ellipsoid with most of its loops and helices exposed to the solvent. A search for proteins with similar structures yielded no matches.

Table 1. Structure determination and statistics. Arp2/3 complex was purified from bovine thymus (*29*) and concentrated to 5 mg/ml by ion-exchange chromatography in 20 mM tris (pH 8.0), 100 mM NaCl, 1 mM EGTA, 1 mM $MgCl_2$, and 1 mM dithiothreitol. The protein crystallized in 1 to 3 days at 4°C by vapor diffusion against 6% polyethylene glycol (PEG) 8000, 0.1 M KSCN, and 0.1 M Hepes (pH 7.5). Large crystals obtained by macro seeding were soaked in 18% PEG 8000, 20% glycerol, 0.2 M KSCN, and 0.1 M Hepes for 1 hour and flash-frozen in liquid N_2. The Pt derivative was obtained by soaking the crystal in the cryoprotection buffer with 10 mM $KPtNO_2$ for 24 hours. Diffraction data from frozen crystals (100 K) were measured with a charge-coupled device detector on beamline 9-2, Stanford Synchrotron Radiation Laboratory (Palo Alto, CA) using oscillations less than 0.5° to avoid overlaps due to the large cell dimensions. Reflection data were indexed and integrated using MOSFLM and scaled using SCALA (*36*). Initial Pt sites were observed in anomalous Patterson maps, and eight sites were identified using SOLVE (*36*). MLPHARE identified and refined 34 Pt sites per asymmetric unit. Phases calculated with MLPHARE were solvent-flattened using DM on the basis of a solvent content of 58% (one complex per asymmetric unit). Electron density maps showed clear elements of secondary structure. An automated search of the maps with actin (1ATN) using FFFEAR did not locate the Arp2 or Arp3. However, searching with the small (residues 4 to 145) and large (residues 147 to 334) domains separately identified the position of Arp3 and the large domain of Arp2. Upon recognition of the β-propeller structure of p40, the alanine backbone of the G protein β subunit (1GP2) was placed into the density as an initial model. Additional secondary structure elements were identified and built manually (*37*). The amino acid sequences of the seven bovine subunits came from expressed sequence tag databases. The first round of refinement included 65% of the residues. The present model resulted from three more rounds of rebuilding and refinement (*38, 39*).

	Pt λ1	Pt λ2	Pt λ3	Native
Space group	$P2_12_12_1$			$P2_12_12_1$
Unit cell dimensions (Å)	a = 110.84, b = 129.64, c = 201.35			a = 111.71, b = 130.40, c = 204.93
Wavelength (Å)	1.07223	1.07159	0.84340	1.08
Resolution (Å)	80–2.7	80–2.7	80–2.8	20–2.01
Reflections	245,352	277,251	247,302	852,046
Unique reflections	70,413	78,496	70,583	183,319
Redundancy	3.5	3.5	3.5	4.6
Completeness (%)	98.0	98.8	98.5	92.8
$I/\sigma(I)$*	12.7	11.1	12.2	8.6
R_{merge}	4.3	4.3	4.4	6.4
Refinement statistics				
Residues				1709
Non-hydrogen atoms				15,600
Protein non-hydrogen atoms				13,582
R_{crys}				21.6%
R_{free}†				24.9%
RMS deviation bonds				0.011 Å
RMS deviation angles				1.353°
Mean temp. factor				35.7

*$I/\sigma(I)$ is the ratio of diffraction intensity to its variance. †$R_{free} = \Sigma(F_{obs} - F_{calc})/\Sigma(F_{obs})$ calculated for 5% of the data not used for treatment.

Inactive and active conformations of the Arp2/3 complex. Highly purified bovine Arp2/3 complex is inactive with respect to actin filament nucleation unless stimulated by WASp/Scar proteins and actin filaments (*29*). Assuming that the Arps form the first two subunits in the new actin filament (*19, 21, 22*), the arrangement of the Arps in the purified complex explains why it is inactive. Although the Arps lie approximately head to tail like subunits in the long-pitch helix of an actin filament, they are rotated 180° around the filament axis relative to each other (Fig. 4, A and B). Thus, the Arps form neither a long-pitch actin helix nor a short-pitch actin helix (Fig. 4C).

We propose that ATP binding to the Arps

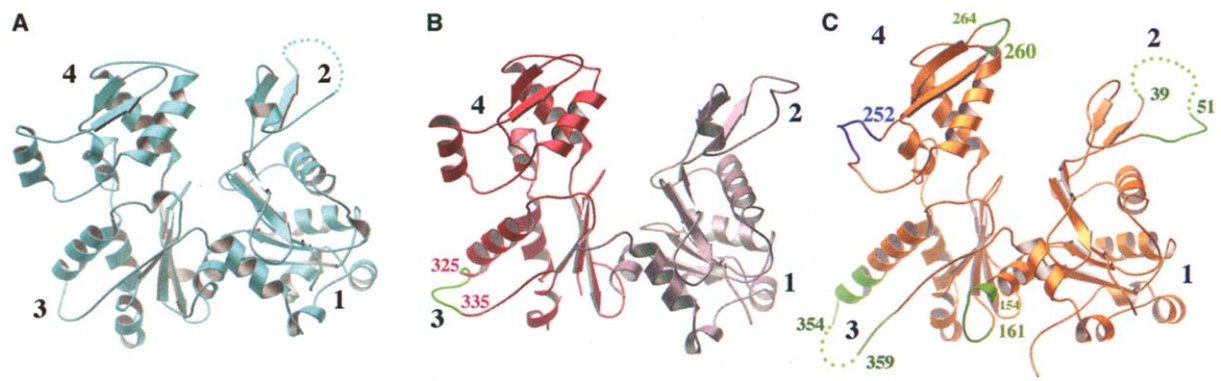

Fig. 2. Ribbon diagrams comparing actin and the two Arps in the Arp2/3 complex. (**A**) Rabbit skeletal muscle actin from the cocrystal with DNase I (PDB accession number 1ATN). (**B**) Arp2. Subdomains 3 and 4 are the refined model consisting of residues Gly^{154} to Arg^{343}. The backbone of actin subdomains 1 and 2 (shaded gray-red) is positioned according to the experimental density of the α helices in the refined map of the Arp2/3 complex. The insert Tyr^{325}-Glu^{335} in subdomain 3 is colored green. (**C**) Arp3. The major inserts (Gln^{46} to Cys^{54}, Thr^{154} to Arg^{161}, Asn^{260} to Lys^{264}, and Val^{347} to Leu^{358}) are colored green. Residues 40 to 50 do not appear in the electron density map.

and a modest rigid-body rotation rearranges the Arp2/3 complex into a conformation that favors nucleation of a new filament (Fig. 4D). Nucleotide binding presumably closes the open clefts of Arp2 and Arp3. A rotation of about 20° of Arp2, p20, p40, and p16 relative to Arp3, p34, and p21 would translate Arp2 ~3 nm relative to Arp3, positioning subdomain 4 of Arp2 next to subdomain 3 of Arp3 exactly like a short-pitch actin dimer. A variety of intersubunit or intrasubunit movements could achieve this docking of the Arps without producing clashes between the subunits. Given the stability of the complex (*20*), we view this class of rotations to be more likely than other rearrangements involving subunit dissociation and rebinding, such as rotation of Arp2 180° around its pointed end–barbed end axis to form an Arp dimer similar to a long-pitch helix dimer of an actin filament. Incorporating one Arp into the barbed end of a preexisting filament and the other into a branch (*20*) would also require a massive rearrangement of subunits.

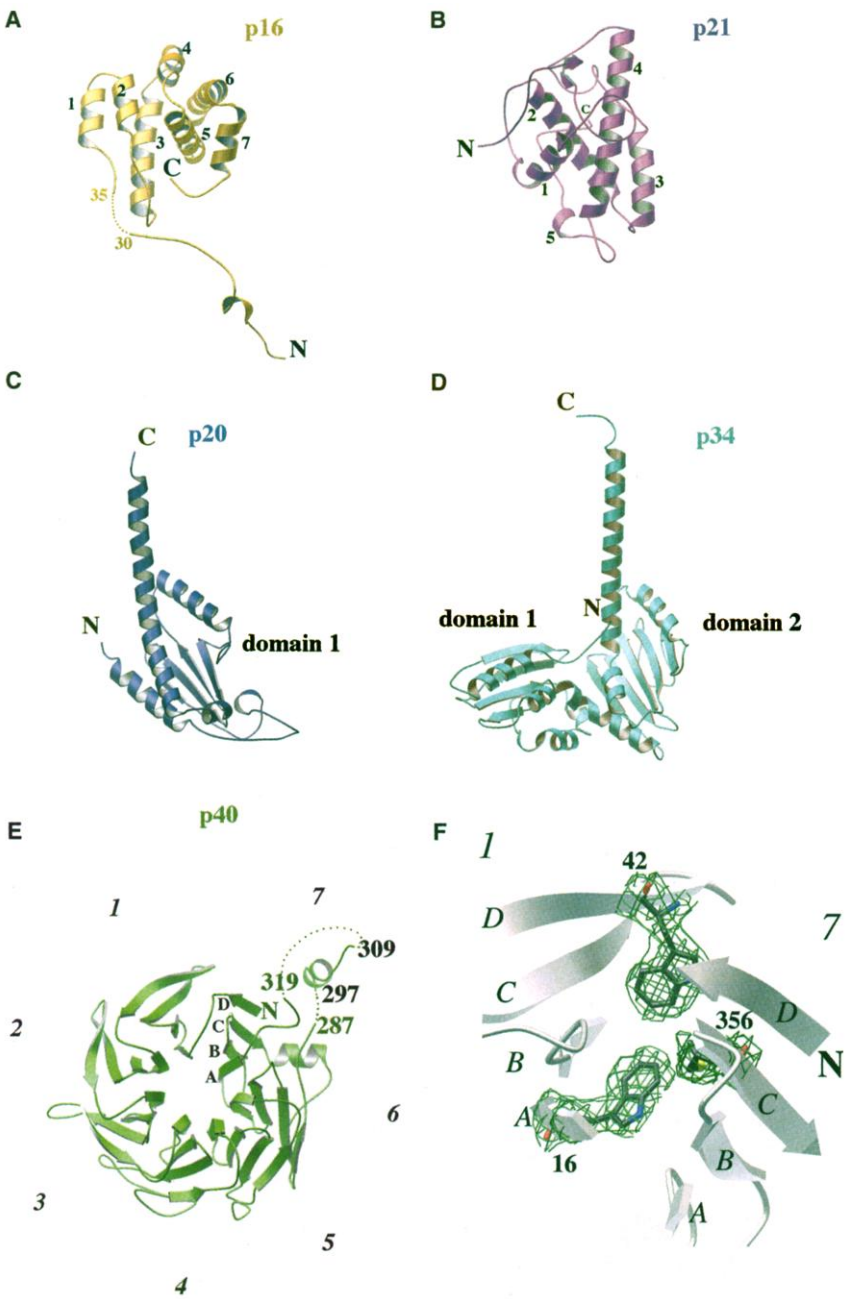

Fig. 3. Ribbon diagrams of the other individual subunits of the Arp2/3 complex. (**A**) ARPC5 p16 with the seven α helices indicated. (**B**) ARPC3 p21 with the five α helices indicated. (**C**) ARPC4 p20 with the NH_2-terminal α/β domain indicated. (**D**) ARPC2 p34 with the NH_2-terminal α/β1 and α/β2 indicated. (**E**) ARPC1 p40 with the seven blades indicated around the edge and the four strands of blade 7 marked A, B, C, and D. Residues 289 to 296 and 310 to 319 do not appear in the electron density map. (**F**) Detail of p40 with the same orientation as (E), showing $3F_{obs} - 2F_{calc}$ electron density maps contoured at the 1σ level around residues Trp^{16}, Trp^{42}, and Met^{356}.

The proposed compact conformation leaves both the barbed and pointed ends of the Arp dimer relatively exposed, such that the Arp dimer could, in principle, elongate at either end or even fit into the middle of an actin filament. However, incorporating the Arp2/3 complex into the middle of a filament would leave no obvious nucleation site for the daughter filament and is inconsistent with both biochemical (*4–6*) and electron microscopic data (*21*). In particular, Arp2/3 complex binds to and initiates branches from the sides of preformed actin filaments, even if these mother filaments are stabilized by phalloidin (*5, 6*). Therefore, we favor the view that Arp2/3 complex binds to the side of the mother filament and that the Arps are the first two subunits in the branch (*21*).

Nucleation of barbed end growth by Arp2/3 complex. Arp2 appears to be unobstructed and suitable for addition of an actin subunit at either its barbed or pointed end. Both ends of Arp3 appear to be generally compatible with polymerization, except for insertions that would interfere at both ends: residues 259 to 265 at the pointed end and residues 347 to 362 at the barbed end. Thus, the barbed end of Arp3 is more obstructed and the pointed end less obstructed than predicted (*19*).

Rearrangements of surface loops are likely to be required for elongation from either the barbed end or the pointed end of Arp3. The favored end is not obvious on structural grounds, but filament branches nucleated by Arp2/3 complex grow in the barbed direction both in vitro (*4, 5, 21*) and in cells (*2, 3*). Perhaps the activation process favors rearrangement of the obstructing surface features at the barbed end relative to the pointed end. Alternatively, faster elongation at the barbed end may simply overwhelm slow growth at the pointed end, particularly in cells where profilin prevents pointed end growth.

Activation of Arp2/3 complex. We suggest that all factors known to promote nucleation by Arp2/3 complex do so by favoring the same active conformation. The known nucleation-promoting factors are proteins related to WASp [reviewed in (*13*)], preexisting actin filaments (*5, 6, 29, 30*), and ATP (*27*). WASp and related proteins stimulate nucleation by Arp2/3 complex, but only after a lag. Filaments eliminate this lag, which suggests that filaments formed during the lag promote nucleation autocatalytically. Thermodynamic coupling between the binding of WASp and actin filaments to Arp2/3 complex (*14*) suggests that both ligands favor the same active conformation of Arp2/3 complex. New evidence suggests that ATP binding and hydrolysis by Arp2/3 complex also promotes nucleation (*27*), perhaps by favor-

ing closure of the nucleotide-binding clefts of Arp2 and Arp3 that we propose to be part of the change to the compact conformation.

An attractive mechanism is that nucleation-promoting factors stabilize the compact conformation by bridging p40 and p21. The active part of WASp (and related proteins such as N-WASP and Scar) consists of three named segments, W, C, and A. The 19-residue WH2 domain (W or V for verprolin homology) binds monomeric actin in much the same way that profilin binds actin (*11, 29*). A central segment (C) of 37 residues contributes to binding both actin and Arp2/3 complex (*14*). The COOH-terminal acidic segment (A) of 18 residues (13 of which are acidic) binds p21, as judged from two hybrid interactions (*15*). C and A are required for activation, and N-WASP WCA can be chemically cross-linked to Arp3, Arp2, p40, and p21 (*31*). WH2 does not bind Arp2/3 complex (*14*) but is postulated to contribute to activation by anchoring the first actin subunit in the new filament to Arp2/3 complex (*15*). This is expected to be an effective strategy for promoting nucleation, because actin trimers are very unstable as a result of rapid dissociation (*12*).

Filament branching. Preexisting actin filaments not only form the base for Arp2/3 complex to anchor a 70° branch, they also cooperate with WASp/Scar proteins to activate Arp2/3 complex. Arp2/3 complex has a low affinity for the sides of actin filaments, but binding to filaments enhances the affinity of WCA for Arp2/3 complex (*14*). This thermodynamic coupling is most simply explained by binding of filaments and WCA each favoring the active conformation. Analysis of electron micrographs of frozen-hydrated branches (*21*) shows that Arp2/3 complex contacts three successive subunits along one long-pitch helix of the mother filament and suggests that the Arps form the first two subunits of the branch. The actin subunits of the mother filament are completely unperturbed at the branch (*21*).

Subunits p34 and p40 are leading candidates to anchor the complex to the side of the mother filament. Chemical cross-linking (*20, 22*) and inhibition of branching by an antibody to p34 (*32*) both indicate that p34 contacts the mother filament. A structural argument implicates p40. A helix in the loop between blades 6 and 7 of p40 contacts Arp3 in an adjacent complex [Web fig. 2A (*23*)]. Helices of gelsolin (*33, 34*) and profilin (*35*) contact a similar nonpolar surface between subdomains 1 and 3 of actin [Web fig. 2B (*23*)]. Anchoring the helix in the p40 loop on a subunit in an actin filament would position the complex on the side of the filament. However, rotation of the entire complex 180° relative to its position in the crystal would be required to orient the barbed end of the branch correctly with respect to the polarity of the mother filament. The disordered loops

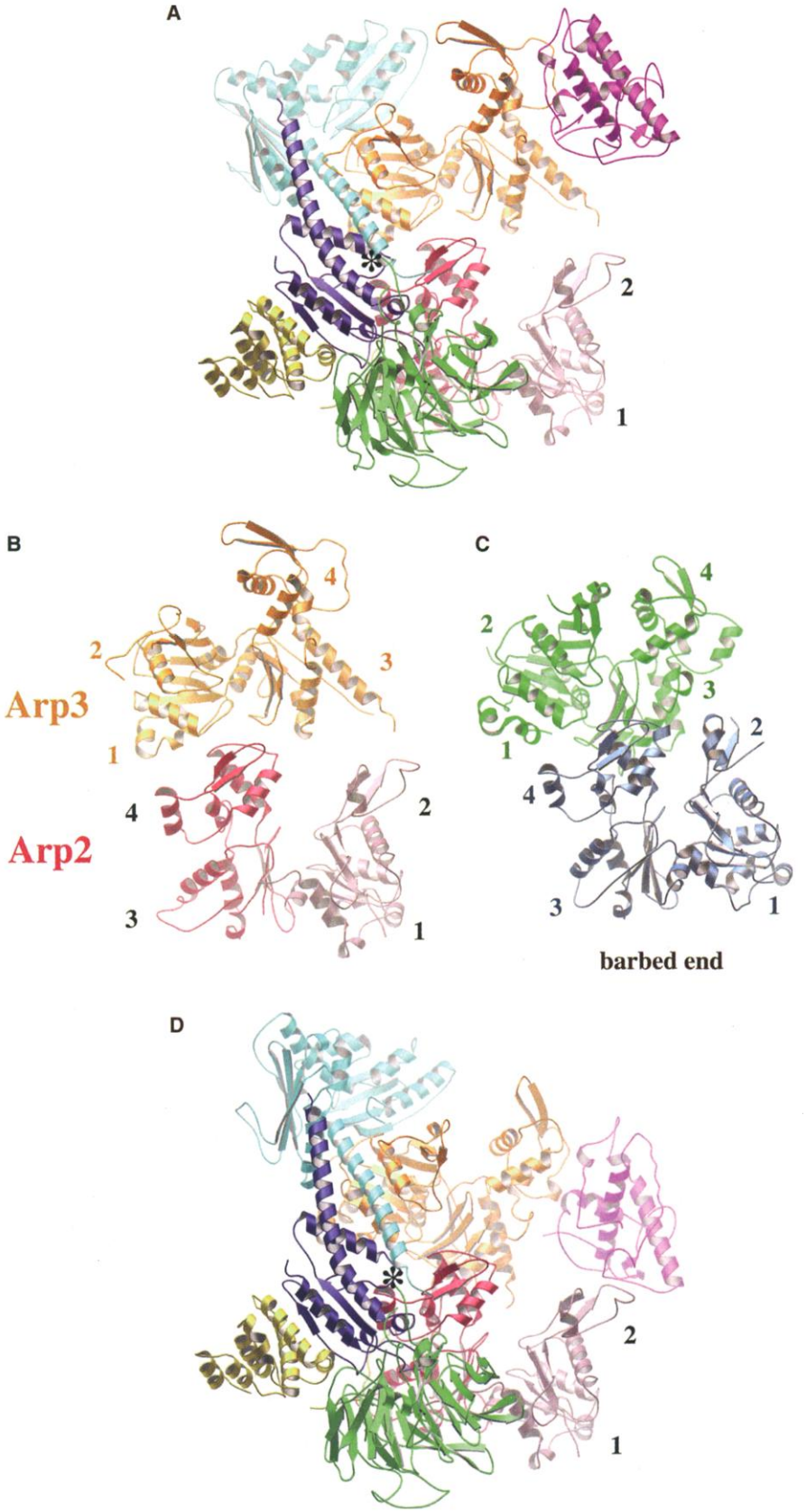

Fig. 4. Model for activation of Arp2/3 complex: ribbon diagrams of (**A**) the inactive complex, (**B**) the Arps in the inactive complex, (**C**) a short-pitch actin dimer from an actin filament, and (**D**) the proposed active complex. In (D), Arp2, p20, p40, and p16 were shifted as a rigid body so that Arp2 contacts Arp3 like two subunits of a short-pitch actin filament helix. The asterisk marks the approximate position of the loop between blades 6 and 7.

connecting the p40 "anchoring helix" to Arp3 may allow this reorientation.

Much more work is required to determine how Arp2/3 complex is activated and mediates filament branching. The crystal structure of Arp2/3 complex provides the foundation for detailed analysis of these mechanisms as well as more penetrating studies of actin filament dynamics in cells.

References and Notes

1. L. M. Machesky, S. J. Atkinson, C. Ampe, J. Vandekerckhove, T. D. Pollard, *J. Cell Biol.* **127**, 107 (1994).
2. T. M. Svitkina, A. B. Verkhovsky, K. M. McQuade, G. G. Borisy, *J. Cell Biol.* **139**, 397 (1997).
3. T. M. Svitkina, G. G. Borisy, *J. Cell Biol.* **145**, 1009 (1999).
4. R. D. Mullins, J. A. Heuser, T. D. Pollard, *Proc. Natl. Acad. Sci. U.S.A.* **95**, 6181 (1998).
5. L. Blanchoin *et al.*, *Nature* **404**, 1007 (2000).
6. K. J. Amann, T. D. Pollard, *Nature Cell Biol.* **3**, 306 (2001).
7. L. M. Machesky *et al.*, *Proc. Natl. Acad. Sci. U.S.A.* **96**, 3739 (1999).
8. R. Rohatgi *et al.*, *Cell* **97**, 221 (1999).
9. D. Winter, T. Lechler, R. Li, *Curr. Biol.* **9**, 501 (1999).
10. D. Yarar, W. To, A. Abo, M. D. Welch, *Curr. Biol.* **9**, 555 (1999).
11. C. Egile *et al.*, *J. Cell Biol.* **146**, 1319 (1999).
12. T. D. Pollard, L. Blanchoin, R. D. Mullins, *Annu. Rev. Biophys. Biomol. Struct.* **29**, 545 (2000).
13. H. N. Higgs, T. D. Pollard, *Annu. Rev. Biochem.* **70**, 649 (2001).
14. J. B. Marchand, D. A. Kaiser, T. D. Pollard, H. N. Higgs, *Nature Cell Biol.* **3**, 76 (2001).
15. L. M. Machesky, R. H. Insall, *Curr. Biol.* **8**, 1347 (1998).
16. H. Miki, T. Takenawa, *Biochem. Biophys. Res. Commun.* **243**, 73 (1998).
17. L. M. Machesky *et al.*, *Biochem. J.* **328**, 105 (1997).
18. M. D. Welch, A. H. DePace, S. Verma, A. Iwamatsu, T. J. Mitchison, *J. Cell Biol.* **138**, 375 (1997).
19. J. F. Kelleher, S. J. Atkinson, T. D. Pollard, *J. Cell Biol.* **131**, 385 (1995).
20. R. D. Mullins, W. F. Stafford, T. D. Pollard, *J. Cell Biol.* **136**, 331 (1997).
21. N. Volkmann *et al.*, *Science* **293**, 2456 (2001).
22. R. D. Mullins, T. D. Pollard, *Curr. Opin. Struct. Biol.* **9**, 244 (1999).
23. For supplemental information, see *Science* Online (www.sciencemag.org/cgi/content/full/294/5547/1679/DC1).
24. D. C. Winter, E. Y. Choe, R. Li, *Proc. Natl. Acad. Sci. U.S.A.* **96**, 7288 (1999).
25. The arrangement of subunits agrees well with the following contacts identified by chemical cross-linking: Arp3 to p34, p21, and p20; Arp2 to p40 and p34 (long linker); p40 to p34; and p20 to p16 (long linker). It also agrees with a two-hybrid interaction, p34 to p20 (*15*).
26. The residues of Arp2 that interact with ATP in actin are highly conserved in Arp2: actin Asp^{154} = Arp2 Asp^{158}, Asp^{157} = Asp^{161}, Gly^{158} = Gly^{162}, Val^{159} = Val^{163}, Lys^{213} = Lys^{217}, Glu^{214} = Glu^{218}, Gly^{301} = Gly^{306}, Thr^{302} = S^{307}, Met^{304} = Met^{309}, and Tyr^{305} = Tyr^{310}. The residues of Arp3 that interact with ATP in actin are also highly conserved: actin Asp^{11} = Arp3 Asp^{11}, Ser^{14} = Thr^{14}, Gly^{15} = Gly^{15}, Leu^{16} = Tyr^{16}, Lys^{18} = Lys^{18}, Asp^{154} = Asp^{169}, Asp^{157} = Asp^{172}, Gly^{158} = Gly^{173}, Val^{159} = Val^{174}, Lys^{213} = Lys^{228}, Glu^{214} = Glu^{229}, Gly^{301} = Gly^{324}, Thr^{302} = Ser^{325}, Met^{304} = Met^{327}, Tyr^{305} = Phe^{328}, and Lys^{336} = Arg^{374}.
27. M. J. Dayel, E. A. Holleran, R. D. Mullins, *Proc. Natl. Acad. Sci. U.S.A.*, in press.
28. The following residues contribute to the interface between the COOH-terminal helices of p34 and p20: p34 Leu^{243}, Phe^{247}, Tyr^{250}, His^{254}, Ser^{258}, Tyr^{261}/Ile^{262}, Phe^{273}, Val^{276}/Leu^{277}; p20 Phe^{134}, His^{137}, Met^{149}, Ser^{152}, Arg^{156}, Val^{160}, and Phe^{164}. Two salt bridges between the helices are p34 Arg^{265}–p20 Glu^{145} and p34 Lys^{296}–p20 Glu^{141}. Rather than a 3-4-3-4-3-4 pattern, the pattern of interface residues is 4-3-4-4-4-3-4-4-3 in p34 and 3-4-4-4-3-4-4-4 in p20. Two interface residue pairs of p34 (Tyr^{261}/Ile^{262} and Val^{276}/Leu^{277}) straddle the p20 chain.
29. H. N. Higgs, L. Blanchoin, T. D. Pollard, *Biochemistry* **38**, 15212 (1999).
30. D. Pantaloni, R. Boujemaa, D. Didry, P. Gounon, M.-F. Carlier, *Nature Cell Biol.* **2**, 385 (2000).
31. J. Zalevsky, I. Grigorova, R. D. Mullins, *J. Biol. Chem.* **276**, 3468 (2001).
32. M. Bailly *et al.*, *Curr. Biol.* **11**, 620 (2001).
33. P. J. McLaughlin, J. T. Gooch, H. G. Mannherz, A. G. Weeds, *Nature* **364**, 685 (1993).
34. R. C. Robinson *et al.*, *Science* **286**, 1939 (1999).
35. C. E. Schutt, J. C. Myslik, M. D. Rozychi, N. C. Goonesekere, U. Lindberg, *Nature* **365**, 810 (1993).
36. Collaborative Computational Project No. 4, *Acta Crystallogr. D* **50**, 760 (1994).
37. T. A. Jones, J. Y. Zou, S. W. Cowan, M. Kjeldgaard, *Acta Crystallogr. A* **47**, 100 (1991).
38. A. Perrakis, T. K. Sixma, K. Wilson, V. S. Lamzin, *Acta Crystallogr. D* **53**, 448 (1997).
39. E. La Fortelle, G. Bricogne, *Methods Enzymol.* **276**, 472 (1997).
40. DINO: Visualizing Structural Biology (2001) (www.dino3d.org).
41. P. J. Kraulis, *J. Appl. Crystallogr.* **24**, 946 (1991).
42. Persistence of Vision Raytracer (1997) (www.povray.org).
43. A. Nicholls, K. A. Sharp, B. Honig, *Proteins Struct. Funct. Genet.* **11**, 281 (1991).

44. The coordinates are deposited in the Protein Data Bank (PDB) (accession number 1K8K). We thank W. Kwiatkowski for help with the illustrations and computer systems, D. Davies of NIH for providing hospitality for K.T. in Maryland, and K. Amann, E. Andrianantoandro, and C. Beltzner for helpful suggestions on the text. Supported by NIH research grants GM-26132 and GM-26338 (T.P.) and GM-56653 (S.C.), a Pioneer Foundation Fellowship (R.R.), an NRSA Fellowship (H.H.), and the Human Frontier Science Program.

18 September 2001; accepted 25 October 2001

REPORTS

Self-Assembly and Mineralization of Peptide-Amphiphile Nanofibers

Jeffrey D. Hartgerink, Elia Beniash, Samuel I. Stupp*

We have used the pH-induced self-assembly of a peptide-amphiphile to make a nanostructured fibrous scaffold reminiscent of extracellular matrix. The design of this peptide-amphiphile allows the nanofibers to be reversibly cross-linked to enhance or decrease their structural integrity. After cross-linking, the fibers are able to direct mineralization of hydroxyapatite to form a composite material in which the crystallographic c axes of hydroxyapatite are aligned with the long axes of the fibers. This alignment is the same as that observed between collagen fibrils and hydroxyapatite crystals in bone.

Self-assembly and biomineralization are used in biology for fabrication of many composite materials. Bone tissue is a particularly complex example of such a composite because it contains multiple levels of hierarchical organization (*1*). At the lowest level of this hierarchy is the organization of collagen fibrils with respect to hydroxyapatite (HA) crystals. The collagen fibrils are formed by self-assembly of collagen triple helices and the HA crystals grow within these fibrils in such a way that their *c* axes are oriented along the long axes of the fibrils (*2*). The preparation of any material with structure on the nanoscale is a challenging problem. Fabrication of materials that resemble bone, even at the lowest level of hierarchical organization, is even more difficult because it involves two dissimilar organic and inorganic nanophases that have a specific spatial relation with respect to one another. One way to accomplish this in an artificial system is to prepare an organic nanophase designed to exert control over crystal nucleation and growth of the inorganic component.

The controlled nucleation and growth of crystals from organic templates has been demonstrated by in vitro experiments (*3–8*) and in a number of natural biomineralizing systems (*9–11*). These studies on templated crystal growth suggest that nucleation occurs on surfaces which expose repetitive patterns of anionic groups. These anionic groups tend to concentrate the inorganic cations creating local supersaturation followed by oriented nucleation of the crystal. Many groups have investigated the preparation of bone-like materials with the use of organic substrates such as poly(lactic acid), reconstituted collagen, and many others (*12–18*), and some studies show a similar correlation between the crys-

Department of Materials Science and Engineering, Department of Chemistry, and Medical School, Northwestern University, 2225 North Campus Drive, Evanston, IL 60208, USA.

*To whom correspondence should be addressed. E-mail: s-stupp@northwestern.edu